

## Quasi-Phase-Matched Laser Wakefield Acceleration

S. J. Yoon, J. P. Palastro, and H. M. Milchberg

*Institute for Research in Electronics and Applied Physics, University of Maryland, College Park, Maryland 20740, USA*

(Received 28 October 2013; published 3 April 2014)

The energy gain in laser wakefield acceleration is ultimately limited by dephasing, occurring when accelerated electrons outrun the accelerating phase of the wakefield. We apply quasi-phase-matching, enabled by axially modulated plasma channels, to overcome this limitation. Theory and simulations are presented showing that weakly relativistic laser intensities can drive significant electron energy gains.

DOI: 10.1103/PhysRevLett.112.134803

PACS numbers: 41.75.Jv, 52.35.Fp, 52.59.Bi, 52.59.Fn

The ponderomotive force of a high-intensity, ultrashort laser pulse displaces plasma electrons, exciting plasma waves [1]. Realizing that the axial electric field associated with the plasma wave far surpasses that of conventional accelerators, Tajima and Dawson suggested harnessing the wakefield for electron acceleration [2]. Since their seminal paper, the promise of building smaller-scale, cheaper “advanced accelerators” has led to a number of theoretical advances [3–5] and experimental demonstrations [6–9] of laser wakefield acceleration (LWFA). Several groups have recently achieved LWFA energy gains of  $\sim 2$  GeV [10,11]. Without multiple stages, the energy gain in these experiments is ultimately limited by dephasing, where electrons outrun the accelerating phase of the wakefield.

The operating paradigm for recent nonlinear wakefield acceleration experiments is to set the distance over which the laser pulse energy is depleted by driving plasma waves to the dephasing length, the distance over which the accelerated electrons outrun the accelerating phase of the wakefield [10,12]. Because the dephasing length scales as  $L_d \propto n_0^{-3/2}$ , where  $n_0$  is plasma density and the maximum axial field is limited to the plasma wave breaking field,  $E_{\max} \propto n_0^{1/2}$ , lower densities increase the maximum energy gain of electrons:  $\Delta\gamma \propto E_{\max} L_d \propto n_0^{-1}$  [5], where  $\gamma$  is the relativistic factor. The laser pulse must also stay collimated over the dephasing length. Self-guiding, where the transverse ponderomotive force of the laser pulse bores a guiding structure in the plasma, is one solution, but at lower density it requires higher pulse powers,  $P_{sf} \propto n_0^{-1}$  for relativistic self-focusing [5,12]. Alternatively, preformed plasma waveguides [7,13,14] can be used, eliminating the power dependence of the guiding condition.

Axial-density-modulated plasmas [15] have been suggested for plasma accelerator injectors [16,17], quasi-phase-matched direct laser acceleration of electrons [18–21], and terahertz generation [22]. In an axially modulated plasma waveguide [15], the guided mode is composed of spatial harmonics whose associated phase velocities can be tuned by varying the modulation period. Quasi-phase-matching (QPM) refers to matching the phase velocity of an individual spatial harmonic to the electron velocity [18–21].

Here we investigate the application of QPM in modulated plasma channels to LWFA (QPM-LWFA). The frequency of the excited plasma wave, and consequently its phase velocity, undergoes oscillations in the modulated plasma. As a result, the plasma wave itself is composed of spatial harmonics. By matching the modulation period to the dephasing length, a relativistic electron can undergo energy gain over several dephasing lengths. Furthermore, QPM-LWFA can operate at much lower pulse energies and provides a guiding structure for the laser pulse, thus loosening the three energy gain limitations associated with standard LWFA: dephasing, depletion, and diffraction.

We start by examining the electrostatic fields of ponderomotively driven plasma waves in a corrugated plasma channel. The density profile of the plasma is modeled as  $n_e(r, z) = n_0[1 + \delta \sin(k_m z)] + \frac{1}{2} n_0'' r^2$ , where  $n_0$  is the average on-axis density,  $\delta$  is the modulation amplitude,  $k_m = 2\pi/\lambda_m$  is the wave number associated with modulations of period  $\lambda_m$ , and  $n_0''$  describes the curvature of the channel. The transverse parabolic density profile provides guiding for a laser pulse with an  $\exp(-1)$  field radius  $w_{ch} = (2c)^{1/2}(m_e/2\pi e^2 n_0'')^{1/4}$ , where  $c$  is the speed of light in vacuum and  $m_e$  and  $e$  are the electron rest mass and charge, respectively.

To illustrate the concept and to derive a scaling for the energy gain, we consider a weakly relativistic laser pulse propagating along the  $z$  axis with wavelength  $\lambda_0 = 2\pi/k_0$  and normalized vector potential  $\mathbf{a} = e\mathbf{A}/m_e c$ . As the laser pulse propagates through the plasma, its ponderomotive force drives an electron plasma wave with a phase velocity equal to the group velocity of the laser pulse. By using a separation of time scales based on the disparity between the laser pulse and plasma frequencies, the equation for the wakefield in a nonuniform plasma is found from the fluid and Maxwell's equations,

$$\left[ \frac{\partial^2}{\partial \xi^2} + k_p^2(r, z) \right] \mathbf{E} = -\pi e n_e(r, z) \nabla |\mathbf{a}|^2, \quad (1)$$

where  $k_p^2 = \omega_p^2/c^2 = 4\pi e^2 n_e/m_e c^2$  and  $\xi = z - v_g t$  is the coordinate in a frame moving with the group velocity  $v_g$  of

the laser pulse. We are interested in the case of  $\delta \ll 1$  such that  $v_g$  is essentially constant, namely,  $v_g/c \approx 1 - (k_p^2/2k_0^2) - (4/k_0^2 w_{\text{ch}}^2)$ , where  $k_{p0}^2 = \omega_{p0}^2/c^2 = 4\pi e^2 n_0/m_e c^2$ .

We assume a laser pulse of the form  $|\mathbf{a}(\xi, r)|^2 = a_0^2 \exp(-2r^2/w_{\text{ch}}^2) \sin^2(\pi\xi/c\sigma)$  on the domain  $0 < \xi < c\sigma$  with temporal full width at half maximum (FWHM)  $\sigma_{\text{FWHM}} = \sigma/2$  matched to the on-axis plasma period  $\sigma_{\text{FWHM}} = \pi/\omega_{p0}$ . For  $\delta \ll 1$ , the wakefields close to the axis,  $r^2 \ll w_{\text{ch}}^2$ , and after the laser pulse,  $\xi > c\sigma$ , are

$$E_z = -\frac{\pi}{8} a_0^2 \sum_n J_n \left[ \frac{\delta k_{p0}(v_g t - z)}{2} \right] \times \cos \left[ k_{p0} v_g t - (n k_m + k_{p0}) z \right], \quad (2a)$$

$$E_r = -\frac{a_0^2}{2k_{p0} w_{\text{ch}}} \left( \frac{r}{w_{\text{ch}}} \right) \sum_n J_n \left[ \frac{\delta k_{p0}(v_g t - z)}{2} \right] \times \sin \left[ k_{p0} v_g t - (n k_m + k_{p0}) z \right], \quad (2b)$$

where the fields have been normalized to the wave-breaking field  $m_e c \omega_{p0}/e$ . Equations (2) exhibit the decomposition of the wakefields into spatial harmonics whose amplitudes depend on the distance behind the head of the laser pulse and whose phase velocities depend on the modulation period.

Figure 1(a) shows the on-axis longitudinal electric field  $E_z$  of a plasma wave driven by a low amplitude,  $|\mathbf{a}| \ll 1$ ,  $\lambda_0 = 800$  nm laser pulse as a function of  $z - ct$  and  $z$  in a corrugated plasma channel with  $n_0 = 7 \times 10^{18} \text{ cm}^{-3}$ ,  $\delta = 0.04$ ,  $w_{\text{ch}} = 15 \mu\text{m}$ , and  $\lambda_m = 5.0$  mm. The pulse duration and spot are matched to the density and channel curvature, respectively. The wavy lines are the wakefield phase fronts, while the red dashed line marks the path of the on-axis peak of the ( $\sim 10 \mu\text{m}$  long) laser pulse. The pulse slides back in the speed of light frame because  $v_g < c$ . In a uniform channel, the phase fronts are parallel to the group velocity trajectory. In a corrugated channel, the pulse passes through oscillating plasma density, causing the wake phases to oscillate with respect to the pulse trajectory.

From Eqs. (2), the phase velocity  $v_{p,n}$  of the wakefield's  $n$ th spatial harmonic is

$$\frac{v_{p,n}}{c} \approx 1 - \frac{k_{p0}^2}{2k_0^2} - \frac{4}{k_0^2 w_{\text{ch}}^2} - n \frac{k_m}{k_{p0}}. \quad (3)$$

The phase of the  $n$ th spatial harmonic can be made stationary in the speed of light frame by setting the modulation period to  $\lambda_m = -2n\lambda_{p0}^3\lambda_0^{-2}(1 + 8/k_{p0}^2 w_{\text{ch}}^2)^{-1}$ , where  $\lambda_{p0} = 2\pi/k_{p0}$ . For the  $n = -1$  spatial harmonic, this is equivalent to setting the modulation period equal to the dephasing length  $L_d = 2\lambda_{p0}^3\lambda_0^{-2}(1 + 8/k_{p0}^2 w_{\text{ch}}^2)^{-1}$  of standard LWFA. When  $\lambda_m = L_d$ , an electron moving near the

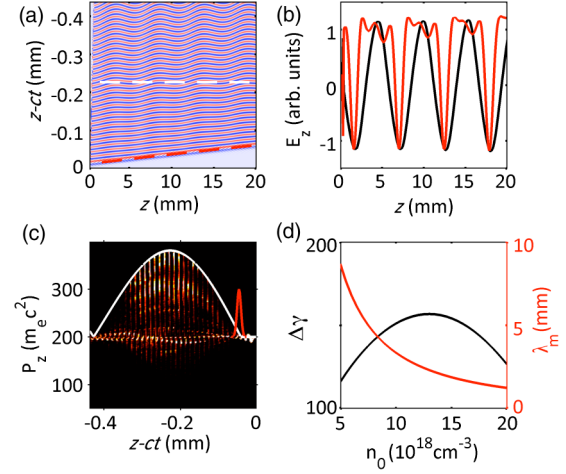


FIG. 1 (color online). (a) On-axis wakefield in a modulated plasma as a function of speed of light frame coordinate  $z - ct$  and axial distance  $z$ . The wavy lines are the plasma wakefield phase fronts, while the red dashed line marks the path of the on-axis peak of the ( $\sim 10 \mu\text{m}$  long) laser pulse. (b) Axial wakefield experienced by an electron moving with an axial velocity near the speed of light at a position marked by the white dashed line in (a). The red and black lines are the fields experienced in a modulated and uniform plasma channel, respectively. (c) Phase space density in the axial momentum speed of light frame plane after 2 mm of interaction. The white line shows the amplitude of the  $n = -1$  spatial harmonic and the red line the envelope of the laser pulse. (d) Predicted energy gain (black, left vertical axis) and matched modulation period (red, right vertical scale) as a function of average on-axis plasma density. Exact parameters are in the text.

speed of light along the channel axis experiences a near constant axial acceleration from the  $n = -1$  spatial harmonic, while the acceleration of all other spatial harmonics time averages to zero.

The red curve of Fig. 1(b) is a lineout along the white dashed curve of Fig. 1(a), in which  $\lambda_m = L_d$ . For comparison, the black curve is a similar lineout for an unmodulated plasma channel. These curves show the longitudinal wakefield acting on an electron moving at nearly  $c$ . In both cases the dominant axial field oscillates at the plasma period, but the oscillations in the modulated channel clearly contain additional harmonics. While the integral of the axial field over a plasma period is zero in the uniform channel, it is nonzero in the modulated channel, showing that the modulated wakefield performs net work on a relativistic electron even after the electron has traversed a full plasma wavelength.

In Fig. 1(c), the phase space of axial momentum,  $P_z$ , and speed of light frame coordinate is plotted for a long, uniform beam of test electrons with an initial axial momentum of 100 MeV/c accelerated over 2 cm. The results were obtained from 2D particle-in-cell simulations which we discuss further below. The pulse amplitude, wavelength, and FWHM were  $a_0 = 0.25$ ,  $\lambda_0 = 800$  nm, and  $\sigma_{\text{FWHM}} = 30$  fs, respectively, and the density parameters

were the same as given above. The red curve indicates the location of the laser pulse propagating to the right in the figure, and the white curve indicates the normalized amplitude of the  $n = -1$  spatial harmonic  $J_{-1}$ . The plot clearly shows that axial momentum gain is proportional to the amplitude of the phase-matched spatial harmonic. The spikes in momentum result from bunching of the positively accelerated electrons in each half-period of the plasma wave.

The energy gain of a relativistic electron accelerated by the phase-matched harmonic can be found by integrating  $d\gamma/dt = -\omega_{p0}(v_z/c)E_z$ , where  $\gamma = [1 + \mathbf{P} \cdot \mathbf{P}/m_e^2 c^2]^{1/2}$  is the electron's relativistic factor. Using Eq. (2a) and setting  $\lambda_m = L_d$ , we find

$$\Delta\gamma(z) \approx \frac{1}{4} \pi a_0^2 \delta^{-1} \frac{k_{p0}}{k_m} \left[ J_0 \left( \frac{1}{2} \delta k_m z + \frac{1}{2} \delta k_{p0} z_0 \right) - J_0 \left( \frac{1}{2} \delta k_{p0} z_0 \right) \right], \quad (4)$$

where  $z_0$  is the initial axial position of an electron and the pulse is initially peaked at  $z = 0$ . The energy gain increases with the laser amplitude through the larger wakefields driven by the pulse. As expected,  $\Delta\gamma(z) \rightarrow 0$  as  $\delta \rightarrow 0$ : Only the  $n = 0$  spatial harmonic is present in this limit. The maximum acceleration will occur for electrons with initial axial positions near the peak of the  $n = -1$  spatial harmonic  $\delta k_{p0} z_0 \sim -4$ . The value for  $\delta$  is, however, limited: Aside from experimental considerations such as density uniformity, the peak of  $J_{-1}$  must occur within the length of the plasma channel,  $L_{ch}$ , such that  $\delta$  can be no smaller than  $\delta_{\min} \sim 4/k_{p0} L_{ch}$ . For  $L_{ch} = 2$  cm and  $n_0 = 7 \times 10^{18}$  cm $^{-3}$ ,  $\delta_{\min} = 4 \times 10^{-4}$ , much smaller than the value of  $\delta = 0.04$  used here.

The energy gain in QPM-LWFA is eventually limited by electrons outrunning the spatial harmonic envelope, the white curve in Fig. 1(c), or pulse evolution and depletion. One can show that for  $n = -1$  and  $\delta \gg \delta_{\min}$ , the length scale for harmonic envelope dephasing is  $L_{-1} = 0.6\delta^{-1}L_d$  for an electron starting at  $z_0 \sim -4/\delta k_{p0}$ . For  $\delta = 0.04$ ,  $L_{-1} = 15L_d$ , an order of magnitude larger than standard LWFA. Based on  $L_{-1}$ , the maximum energy gain of QPM-LWFA is  $\Delta\gamma_{Q,\max} \approx (1/8)[1 - J_0(2)]a_0^2\delta^{-1}k_{p0}L_d$ . Because of the approximate conservation of wave action [23], the pulse depletion length and the length scale for spectral redshifting-induced pulse shape modifications are nearly equal:  $L_{\text{dep}} \sim 4L_d a_0^{-2}$  [4]. By setting  $L_{\text{dep}} = L_{-1}$ , we can estimate the maximum amplitude and energy gain for QPM-LWFA:  $a_{0,\max} \approx 2.6\delta^{1/2}$  and  $\Delta\gamma_{Q,\max} \approx (7/8)[1 - J_0(2)]k_{p0}L_d$ . For  $\delta = 0.04$  this gives  $a_{0,\max} \approx 0.5$  and  $\Delta\gamma_{Q,\max} \approx 170$ , using our earlier parameters. For the same parameters in a uniform plasma, the dephasing-limited energy gain of LWFA is  $\Delta\gamma_{\text{LWFA}} = (\pi/16)a_0^2 k_{p0} L_d \sim 34$ . For both QPM-LWFA and LWFA, the maximum electron energy gain can be increased by

lowering the plasma density. We note that  $\Delta\gamma_{Q,\max}$  underpredicts the energy gain observed in Fig. 1(c). This is somewhat surprising, as the FWHM used for Fig. 1(c) is longer than the matched value used for deriving Eq. (4). As we will see, an enhancement in energy gain results from the nonlinear compression of the laser pulse.

Figure 1(d) displays the modulation period required for phase-matched acceleration by the  $n = -1$  spatial harmonic and the energy gain after 2 cm as a function of plasma density for  $\delta = 0.04$ . The energy initially increases because the wakefield amplitude increases with plasma density. The decrease in energy results from the shortening of the maximum acceleration length due to the inverse density dependence  $k_{p0}L_{-1} \propto n_0^{-1}$ .

Our estimate of the energy gain assumed that the electron's axial velocity was close enough to  $c$  that it did not undergo sufficient phase slippage with respect to the  $n = -1$  spatial harmonic. A condition on the minimum axial momentum for which this assumption is valid, or trapping condition, can be derived from the Hamiltonian of an electron interacting with the  $n = -1$  spatial harmonic. By using  $d\gamma/dt = -\omega_{p0}(v_z/c)E_z$  and defining  $\Phi = k_{p0}v_g t - (k_{p0} + k_m)z$ , the Hamiltonian takes the form

$$H = \frac{1}{8} \pi a_0^2 J_1(2) \sin(\Phi) - \left( \frac{v_g}{c} \right) (\gamma^2 - 1)^{1/2} + \left( 1 - \frac{k_m}{k_{p0}} \right) \gamma, \quad (5)$$

where  $\Phi$  and  $\gamma$  are the conjugate dynamical variables and the electron is assumed to be located near the peak of the spatial harmonic during the trapping process  $J_1[\delta k_{p0}(v_g t - z)/2] \sim J_1(2)$ . Setting  $k_m = 2\pi/L_d$  and using the fact that  $H$  is a constant of the motion, we find the threshold energy for trapping is  $\gamma_{\text{tr},Q} \approx [4J_1(2)E_{\max}]^{-1}$ , where  $E_{\max} = \pi a_0^2/8$ . For  $a_0 = 0.25$ , this predicts a trapping threshold of  $\gamma_{\text{tr},Q} \approx 18$ . For standard LWFA in the linear regime the trapping threshold is given by  $\gamma_{\text{tr},S}/\gamma_g \approx (1 + \gamma_g E_{\max}) - [(1 + \gamma_g E_{\max})^2 - 1]^{1/2}$ , where  $\gamma_g = (1 - v_g^2/c^2)^{-1/2}$  [24]. With the parameters specified earlier, this predicts  $\gamma_{\text{tr},S} \approx 7$ . The increased trapping threshold of QPM-LWFA can be overcome with additional density tailoring to modify the plasma wave's phase velocity and other injection techniques [21,25–27].

Particle-in-cell simulations of quasi-phase-matched laser wakefield acceleration were performed by using TURBOWAVE, fully described elsewhere [28]. The fields, particle trajectories, densities, and currents were calculated on a 2D planar-Cartesian grid in a window moving at  $c$ . The window dimensions were  $77 \mu\text{m} \times 438 \mu\text{m}$  with  $512 \times 16384$  cells in the transverse ( $x$ ) and longitudinal ( $z - ct$ ) directions. The plasma density was ramped up over  $200 \mu\text{m}$ . After the initial ramp, the plasma density followed  $n_e(x, z) = n_0[1 + \delta \sin(k_m z)](1 + n_0' x^2/2)$  with

$n_0 = 7 \times 10^{18} \text{ cm}^{-3}$ ,  $n_0''$  set to guide a linearly polarized Gaussian mode with an  $\exp(-1)$  field radius  $w_{\text{ch}} = 15 \text{ }\mu\text{m}$ ,  $\delta = 0.04$ , and  $\lambda_m = L_d = 5.0 \text{ mm}$ .

The laser pulse was initialized with linear polarization in the  $x$  direction, a sine-squared temporal profile, and a Gaussian transverse profile, with the same parameters as above. The simulations were conducted for pulse amplitudes of  $a_0 = 0.25$  (0.5 TW),  $a_0 = 0.375$  (1.1 TW), and  $a_0 = 0.5$  (1.9 TW): pulse energies of only 14, 32, and 56 mJ. The pulse started with its front edge at the beginning of the plasma. An electron bunch of initial axial momentum  $P_z/m_e c = 30$ , and transverse and longitudinal Gaussian profiles with  $\exp(-1)$  radii of 4 and 8  $\mu\text{m}$ , was initialized with its center  $4/\delta k_{p0} = 200 \text{ }\mu\text{m}$  behind the peak of the laser pulse. The peak bunch density was  $n_b = 3.5 \times 10^{16} \text{ cm}^{-3}$  with a total charge of 11 pC, parameters typical of LWFA experiments [29]. We note that because the laser mode is channel guided and the pulse powers are lower than the critical power for self-focusing [30],  $P_{\text{sf}} = 17(\omega/\omega_{p0})^2 \text{ GW} = 4.2 \text{ TW}$ , differences between our 2D simulations and full 3D simulations are minimal.

Figure 2 displays snapshots of background plasma density, laser intensity, and electron bunch density at propagation distances of 0.3, 2.6, and 5.2 mm for the  $a_0 = 0.25$  pulse. The laser pulse enters the plasma channel and excites a plasma wave, visible as the density oscillations trailing the pulse. As the bunch electrons enter the channel, they evolve in response to the wakefields. By 2.6 mm the bunch electrons have been either laterally deflected or strongly focused. The transverse field of the  $n = -1$  spatial harmonic is also quasi-phase-matched to the electrons. For off-axis electrons, the quasi-phase-matched transverse field provides either focusing or defocusing depending on the electron's initial longitudinal position. Comparing  $E_z$  and  $E_r$  in Eqs. (2), we see that there are longitudinal regions of size  $\lambda_p/4$  where electrons are both axially accelerated and focused. Electrons starting in these favorable regions

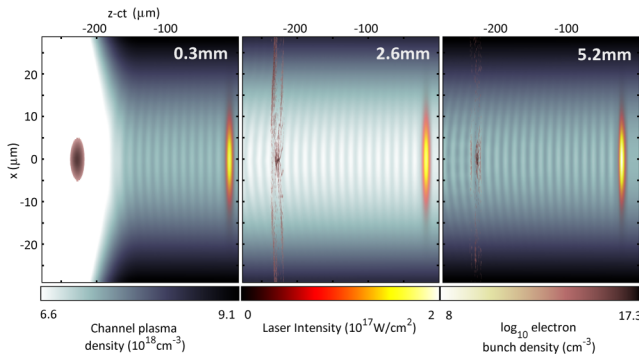


FIG. 2 (color online). Background plasma density, laser pulse intensity, and electron bunch density as a function of transverse position and speed of light frame coordinate at three axial distances: 0.3, 2.6, and 5.2 mm for  $a_0 = 0.25$ . The electron plasma wave is noticeable as the ripples in the background plasma density.

remain on axis and continue to gain energy as they travel behind the laser pulse.

Comparisons of the maximum energy gain resulting from QPM-LWFA and standard LWFA are shown in Fig. 3. When the modulation period is matched to the dephasing length  $\lambda_m = L_d$ , electrons gain energy over several dephasing lengths. In a uniform channel, the electrons initially gain energy but then lose energy as they outrun the accelerating phase of the wake. The energy oscillations in the modulated channel result from the partial deceleration of electrons as they “bucket jump” [31] into the next phase of the plasma wave. After 1.5 cm, the energy gain reaches  $\Delta E \sim 51 \text{ MeV}$  for  $a_0 = 0.25$ , and  $\Delta E \sim 130 \text{ MeV}$  for  $a_0 = 0.375$ , but saturates at  $\Delta E \sim 130 \text{ MeV}$  for  $a_0 = 0.5$ , consistent with our earlier estimate of  $a_{0,\text{max}}$ . When  $a_0 = 0.5$ , nonlinear boring of the plasma density causes the pulse width to oscillate irregularly. As a result, the phase velocity of the plasma wave and hence the dephasing length become nonstationary. The energy gain saturation can be mitigated by varying the modulation period along the channel or by choosing a pulse profile whose spot size varies in time [32].

In spite of the simulation pulse duration being longer than the matched duration, the energy gain for  $a_0 = 0.25$  is nearly that predicted by Eqs. (2). The nonlinear evolution of the laser pulse boosts the acceleration by compressing the initial unmatched pulse duration to a duration closer to the matched value  $\sigma_{\text{FWHM}} \sim \lambda_p/2$  while, at the same time, increasing the wakefield amplitude through the increase in intensity. The pulse's ponderomotive force forms a local nonlinear gradient with the electron density decreasing from the front of the pulse backwards, causing the front and middle of the pulse to undergo spectral redshifting and slide backwards, forming an optical shock [33]. Figure 4 shows the evolution of the pulse's on-axis temporal FWHM and

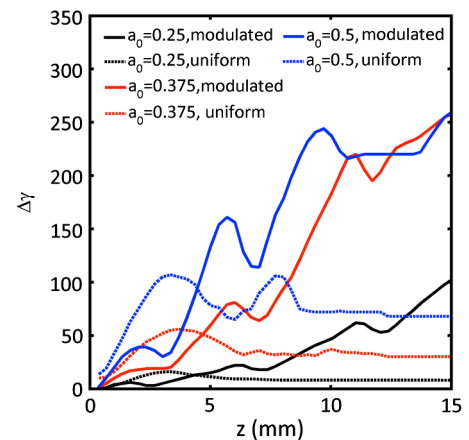


FIG. 3 (color online). Maximum energy gain as a function of distance for electrons with initial axial momentum  $P_z/m_e c = 30$  accelerated in a modulated (solid line) and uniform channel (dashed line). The black, red, and blue lines are for initial pulse amplitudes of  $a_0 = 0.25$ ,  $a_0 = 0.375$ , and  $a_0 = 0.5$ , respectively.

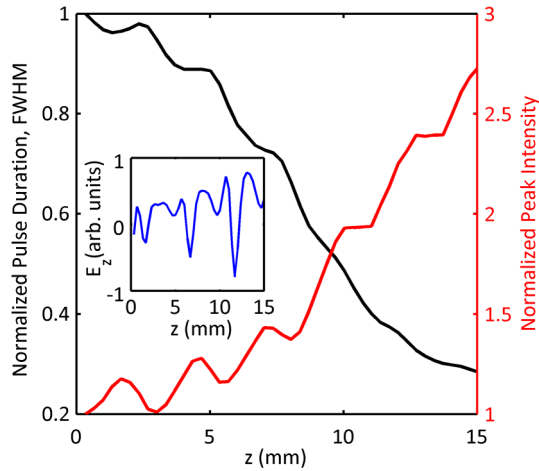


FIG. 4 (color online). On-axis temporal FWHM (black, left vertical axis) and peak intensity (red, right vertical axis) normalized to their initial values as a function of propagation distance. The inset displays the axial wakefield experienced by an electron moving near the speed of light. The wakefield amplitude increases due to the intensity increasing and the pulse duration shortening.

on-axis intensity. Both quantities are normalized to their initial values. The product of FWHM and peak intensity is essentially constant, suggesting that the pulse is not undergoing significant nonlinear focusing or spot oscillations due to unmatched guiding [32]. The inset in Fig. 4 displays the growth in axial wakefield experienced by a relativistic electron in the corrugated channel due to pulse compression.

In conclusion, we have shown that quasi-phase-matching of laser wakefield acceleration, enabled by modulated plasma channels, can overcome the dephasing limitation of standard LWFA. With millijoule level pulses, QPM-LWFA can result in energy gains an order of magnitude higher than LWFA with identical parameters.

The authors thank D. Gordon for the use of TURBOWAVE and continued fruitful collaboration and P. Sprangle for useful discussions. This work was supported by DOE, DTRA, and NSF.

[1] P. Sprangle, E. Esarey, and A. Ting, *Phys. Rev. Lett.* **64**, 2011 (1990).  
 [2] T. Tajima and J. Dawson, *Phys. Rev. Lett.* **43**, 267 (1979).  
 [3] P. Sprangle, E. Esarey, A. Ting, and G. Joyce, *Appl. Phys. Lett.* **53**, 2146 (1988).  
 [4] E. Esarey, C. Schroeder, and W. Leemans, *Rev. Mod. Phys.* **81**, 1229 (2009).  
 [5] W. Lu, M. Tzoufras, C. Joshi, F. Tsung, W. Mori, J. Vieira, R. Fonseca, and L. Silva, *Phys. Rev. ST Accel. Beams* **10**, 061301 (2007).  
 [6] J. Faure, Y. Glinec, A. Pukhov, S. Kiselev, S. Gordienko, E. Lefebvre, J.-P. Rousseau, F. Burgy, and V. Malka, *Nature (London)* **431**, 541 (2004).

[7] C. G. R. Geddes, Cs. Toth, J. van Tilborg, E. Esarey, C. B. Schroeder, D. Bruhwiler, C. Nieter, J. Cary, and W. P. Leemans, *Nature (London)* **431**, 538 (2004).  
 [8] S. P. D. Mangles *et al.*, *Nature (London)* **431**, 535 (2004).  
 [9] B. Hidding *et al.*, *Phys. Rev. Lett.* **96**, 105004 (2006).  
 [10] X. Wang *et al.*, *Nat. Commun.* **4**, 1988 (2013).  
 [11] H. T. Kim, K. H. Pae, H. J. Cha, I. J. Kim, T. J. Yu, J. H. Sung, S. K. Lee, T. M. Jeong, and J. Lee, *Phys. Rev. Lett.* **111**, 165002 (2013).  
 [12] J. E. Ralph, K. A. Marsh, A. E. Pak, W. Lu, C. E. Clayton, F. Fang, W. B. Mori, and C. Joshi, *Phys. Rev. Lett.* **102**, 175003 (2009).  
 [13] C. G. Durfee III and H. M. Milchberg, *Phys. Rev. Lett.* **71**, 2409 (1993).  
 [14] F. Tsung, R. Narang, W. Mori, C. Joshi, R. Fonseca, and L. Silva, *Phys. Rev. Lett.* **93**, 185002 (2004).  
 [15] B. D. Layer, A. York, T. Antonsen, S. Varma, Y.-H. Chen, Y. Leng, and H. Milchberg, *Phys. Rev. Lett.* **99**, 035001 (2007).  
 [16] T. Katsouleas, J. M. Dawson, D. Sultana, and Y. T. Yan, *IEEE Trans. Nucl. Sci.* **32**, 3554 (1985).  
 [17] D. Dahiya, V. Sajal, and A. K. Sharma, *Appl. Phys. Lett.* **96**, 021501 (2010).  
 [18] A. G. York, H. M. Milchberg, J. P. Palastro, and T. M. Antonsen, *Phys. Rev. Lett.* **100**, 195001 (2008).  
 [19] J. P. Palastro and T. M. Antonsen, *Phys. Rev. E* **80**, 016409 (2009).  
 [20] J. P. Palastro, T. M. Antonsen, S. Morshed, A. G. York, and H. M. Milchberg, *Phys. Rev. E* **77**, 036405 (2008).  
 [21] S. J. Yoon, J. P. Palastro, D. Gordon, T. M. Antonsen, and H. M. Milchberg, *Phys. Rev. ST Accel. Beams* **15**, 081305 (2012).  
 [22] A. J. Pearson, J. Palastro, and T. M. Antonsen, *Phys. Rev. E* **83**, 056403 (2011).  
 [23] W. Zhu, J. P. Palastro, and T. M. Antonsen, *Phys. Plasmas* **20**, 073103 (2013).  
 [24] C. B. Schroeder, E. Esarey, B. A. Shadwick, and W. P. Leemans, *Phys. Plasmas* **13**, 033103 (2006).  
 [25] P. Sprangle, J. R. Peñano, B. Hafizi, R. F. Hubbard, A. Ting, D. F. Gordon, A. Zigler, and T. M. Antonsen, *Phys. Plasmas* **9**, 2364 (2002).  
 [26] A. Pak, K. A. Marsh, S. F. Martins, W. Lu, W. B. Mori, and C. Joshi, *Phys. Rev. Lett.* **104**, 025003 (2010); C. McGuffey *et al.*, *Phys. Rev. Lett.* **104**, 025004 (2010).  
 [27] J. Faure, C. Rechatin, A. Norlin, A. Lifschitz, Y. Glinec, and V. Malka, *Nature (London)* **444**, 737 (2006).  
 [28] D. F. Gordon, *IEEE Trans. Plasma Sci.* **35**, 1486 (2007).  
 [29] D. H. Froula *et al.*, *Phys. Rev. Lett.* **103**, 215006 (2009).  
 [30] G. Z. Sun, E. Ott, Y. C. Lee, and P. Guzdar, *Phys. Fluids* **30**, 526 (1987).  
 [31] A. Ting, D. Gordon, M. Helle, D. Kaganovich, P. Sprangle, B. Hafizi, Steven H. Gold, and Gregory S. Nusinovich, *AIP Conf. Proc.* **1299**, 203 (2010).  
 [32] C. Benedetti, C. B. Schroeder, E. Esarey, and W. P. Leemans, *Phys. Plasmas* **19**, 053101 (2012).  
 [33] J. Schreiber, C. Bellei, S. P. D. Mangles, C. Kamperidis, S. Kneip, S. R. Nagel, C. A. J. Palmer, P. P. Rajeev, M. J. V. Streeter, and Z. Najmudin, *Phys. Rev. Lett.* **105**, 235003 (2010).